A&A 420, 371–382 (2004)
DOI: 10.1051/0004-6361:20034214

Astronomy & Astrophysics

The gas and dust coma of Comet C/1999 H1 (Lee)⋆

L.-M. Lara[1], R. Rodrigo[1], G. P. Tozzi[2], H. Boehnhardt[3], and P. Leisy[4]

[1] Instituto de Astrofísica de Andalucía, CSIC, PO Box 3004, 18080 Granada, Spain
e-mail: rodrigo@iaa.es
[2] INAF, Osservatorio Astrofisico di Arcetri, Largo E. Fermi 5, 50125 Firenze, Italy
e-mail: tozzi@arcetri.astro.it
[3] Max-Planck-Institut für Astronomie, Königstuhl 17, 69117 Heidelberg, Germany
e-mail: hboehnha@mpia-hd.mpg.de
[4] Isaac Newton Group of Telescopes, PO Box 321, 38700 Santa Cruz de La Palma, Tenerife, Spain
e-mail: pleisy@ing.iac.es

Received 20 August 2003 / Accepted 19 February 2004

Abstract. Comet Lee (C/1999 H1) was observed on June 6, 1999 when it was at r_h = 0.98 AU and Δ = 1.195 AU. The spectrophotometric observations, between 0.6 and 1 μm, were aimed at the detection of the CI(^{1}D) doublet $\lambda\lambda$ 9823/9850 Å. The non-detection of these lines, with a 3σ flux upper limit of the order of 4.6×10^{-17} erg cm^{-2} s^{-1}, confirms the CO depletion already noted by other authors. Several CN and NH_2 emission bands lie in that spectral range, making it possible to derive production rates for both species as $\sim 3.1 \times 10^{26}$ s^{-1} and 1.2×10^{27} s^{-1}, respectively. The oxygen forbidden line at 6300 Å was used to obtain $Q_{H_2O} = (1.22 \pm 0.7) \times 10^{29}$ s^{-1}. Assuming that CN and NH_2 are directly produced by HCN and NH_3, Comet Lee has a HCN/$H_2O \approx 0.25\%$ and $NH_3/H_2O \approx 1\%$ at r_h = 0.98 AU, in reasonable agreement with what has been found in other long-period comets. The structural analysis carried out on cometary images acquired with broad band *R* Bessel filter clearly displays two pairs of ion rays likely produced by the H_2O^+ doublet at 6198 and 6200 Å, wavelengths covered by the bandpass filter. Identical features are found in the images acquired with the Gunn *i* filter.
The dust brightness profiles in the east-west direction do not deviate from a ρ^{-m} law (with $0.7 < m \leq 1.2$) as expected for a steady state model coma with a constant dust production rate and expanding at constant velocity. The dust production rate, as obtained from the $Af\rho$ parameter, is ∼500 cm, which compared with the gas production rate classifies this comet as a dust poor one with relatively high (6.5–11.7) gas-to-dust mass ratio. Analysis of the normalized reflectivity gradient (i.e. continuum color) as a function of ρ indicates a slight reddening of the solid component in the coma at large cometocentric distances, whereas the average dust color within an aperture of 20 000 km, centered at the nucleus, is ∼9% per 1000 Å. Mie scattering computations applied to an ensemble of particles indicate that the dust coma is characterised by a relative broad size distribution with a typical mean size of 1 μm. These grains might be composed of a mixture of silicates and icy material.

Key words. comets: individual: Comet C/1999 H1 (Lee) – comets: general

1. Introduction

Comet C/1999 H1 (Lee) was discovered on April 16, by Steven Lee from South Wales (IAUC 7144). Subsequent determination of the orbital elements by Marsden (MPEC 1999-H06) classified this new object as a long-period (∼81 000 yr) comet in a "parabolic" orbit (e = 0.999742854) with semimajor axis at 2754 AU.

After discovery, as the comet would reach relatively short geocentric distance when approaching the perihelion, an extensive observation campaign took place. Weaver et al. (1999) carried out pre-perihelion infrared observations of Comet Lee detecting several bands of ethane, from which they estimated a production rate of $(0.7–1.4) \times 10^{27}$ s^{-1} on UT May 20.3, when the comet was at r_h = 1.22 AU and Δ = 0.86 AU. For the same date, the methane production rate was $\sim 4.5 \times 10^{26}$ s^{-1}. Later on, during UT 20–29 May ($1.10 \leq r_h \leq 1.24$ AU, $0.84 \leq \Delta \leq 1.02$ AU), strong emissions were detected in the C–H stretch region near 3.4 μm and also broad emission feature centered near 3.27 μm likely associated with PAHs. The methanol emission at 3.51 μm made it possible to derive a production rate of the order of 2×10^{27} s^{-1}. During this observation campaign, no day-to-day temporal variability was observed at the 20% level.

Mumma et al. (2001) observed the comet in the near-IR (1–5.5 μm) on June 2–3 and on August 19–21, 1999, before and after perihelion, searching for certain key organic species. Molecules such as water, carbon monoxide, methanol, methane, ethane, acetylene and hydrogen cyanide were detected and their production rates derived. The relative abundances found in this survey are similar to those found for

Send offprint requests to: L. M. Lara, e-mail: lara@iaa.es
⋆ Based on observations obtained at ESO La Silla within programme No. 60.A–9011(A).

comets Hyakutake and Hale-Bopp (two other comets that probably had their origin in the nebular region of the giant planets), excepting CO, which is deficient in comet Lee by a factor of 5–10. This CO deficiency demonstrates that chemical diversity occurred within the formation region of the Oort-cloud comets.

Feldman et al. (1999) observed the comet pre-perihelion on June 7, 1999 making use of the Space Telescope Imaging Spectrograph (STIS) installed on the Hubble Space Telescope. The acquired long-slit spectra over the range 115–320 nm with a spatial resolution along the slit of 44 km projected at the comet showed strong emissions due to OH, CS and continuum. The low dust/gas ratio implied by the relative brightness of OH to continuum also enabled the authors to detect S_2 and C_2. Therefore, Comet Lee is the third comet out of four where S_2 has been positively identified (the other three are comet IRAS-Araki-Alcock C/1983 H1, Hyakutake C/1996 B2, and 153P/Ikeya-Zhang). The spatial profiles of CS and the continuum vary in time and are symmetric about the nucleus, while those of the OH bands display significant asymmetry.

Water was also observed with the *Submillimeter Wave Astronomy Satellite*, SWAS, (Melnick et al. 2000) by Nuefeld et al. (2000) on May 19–23, 1999. The production rate derived by these authors (8×10^{28} s^{-1}) is 50% lower than that derived by Biver et al. (2002) from contemporaneous radio observations of hydroxyl molecules. The data, taken over a period of 4.68 days, provide no evidence for variability. Post-perihelion observations, spanning from Sep. to Dec. 1999, with the same satellite (SWAS) (Chiu et al. 2001) indicate that the water production rate was steeply decreasing with heliocentric distance (as $r_h^{-5.5}$ in the range $r_h = 1.3{-}1.7$ AU) and was undetectable after Sep. 28.

In this paper, we present the morphological analysis of broadband images acquired in *R*#642 and *i*#705 filters, after bias and flat field correction as well as sky subtraction. The analysis of spectrophotometric observations of Comet Lee between 0.6 and 1.0 μm taken on June 6, 1999 is also discussed. Two consecutive spectra were acquired aiming at the detection of the CI(^{1}D) doublet at 9823.4 and 9849.5 Å. These spectra also contain information on gas emission from OI(^{1}D), CN and NH_2, and continuum emission due to the scattering of the solar light by the cometary dust grains. Thus, we have obtained CN and NH_2 production rates by using the customary Haser modeling (Haser 1957), H_2O production rate by means of the OI(^{1}D) prompt emission at 6300 Å, and 3σ upper limit detection of the atomic carbon lines. Additionally, we have studied the continuum brightness profiles, the dust color as a function of projected cometocentric distance, ρ and the dust production rate parameterized by $Af\rho$ (A'Hearn et al. 1984). Mie-scattering modeling has provided us with an approximate dust size distribution as well as quantitative composition.

2. Observations and basic data reduction

2.1. Broadband imaging

Comet C/1999 H1 (Lee) was observed at the European Southern Observatory, La Silla, Chile, preperihelion on June 6, 1999, when the comet was at 1.195, 0.979 AU geocentric and heliocentric distance, respectively. We used the EFOSC2 instrument mounted on the 3.6 m telescope (2060×2060 pixels, including overscan pixels, pixel size: 0.″157, usable FOV $5.'2 \times 5.'2$). The telescope tracking was set to the proper motion of the comet and the sky conditions were photometric.

For telescope pointing and slit acquisition purposes, the comet was imaged with *R* Bessel (λ_c = 6431 Å, *FWHM* = 1654 Å) and Gunn *i* (λ_c = 7931 Å, *FWHM* = 1256 Å) filters. Additionally, sky flats were acquired with the same filters for bias and flatfield correction of the images. Since the main objective of the observation campaign was to obtain the long-slit spectra, no devoted standard stars were observed with these broadband filters. However, a summary of the EFOSC2 zero points is available at `http://www.ls.eso.org/lasilla/sciops/efosc/docs/Perf_ZeroPtSummary.html` and we have used the Z_p in *R* and *i* for June 6, 1999 to calibrate these broadband images in Af (see Tozzi & Licandro 2002). An approximate sky background level was determined from ring aperture measurements at a distance from the nucleus at which almost no coma light was found. A morphological analysis has also been carried out on the reduced images.

2.2. Long-slit spectrophotometry

Spectrophotometric observations were taken with a grating of 300 lines per mm, a slit width and length of 1″ and ∼5′, respectively. This resulted in an observable spectral range between 6015 Å and 10 300 Å with a wavelength scale of 2 Å per pixel and a spatial scale of $2 \times 0.''157$ per pixel since the data were rebinned in the spatial direction. The slit of the spectrograph was orientated east-west, leading to spatial profiles that lie approximately parallel to the Sun-comet line projected on the plane of the sky (position angle of the Sun (PA) ≈ 112°). For absolute calibration, we obtained observations of the spectrophotometric standard star LTT 7379 ($V = 10^m23$). The two acquired spectra were reduced using the ESO-MIDAS standard reduction context *long* for long-slit spectra. The spectra were bias subtracted, flatfielded, wavelength calibrated (using He-Ar reference spectra), extinction corrected (using the standard extinction curve for La Silla) and finally flux calibrated. The cometary emission barely filled the slit and the sky flux could be determined form the edges of the frames. Details of the observations are given in Table 1.

3. Data analysis and results

3.1. 2D morphology

Just for completeness, we have investigated the general spatial distribution of particles in the coma of Comet Lee from the acquired broadband images. The analysis of the existing asymmetries was carried out on the images after bias and flatfield correction, and sky subtraction. Either in *R* Bessel or Gunn *i*, the comet shows the dust coma and an incipient dust tail, with a superimposed spherical coma from the gas emission at wavelengths covered by the transmission curve of the filters, as well

Table 1. Details of the observations on June 6, 1999.

Time UT	Band	Exp. time (s)	Δ AU	r_h AU	km per pixel	airmass	PA deg	Phase deg
22:59:33, 23:29:59	Gunn *i*	20				1.76–2.09		
23:07:52–23:51:27	*R* Bessel	20	1.195	0.980	136	1.84–2.20	111.5	54.59
23:40:22–00:06:13	spectra	600				2.30–2.69		

PA refers to the position angle of the extended Sun-target radius vector. Phase is the Sun-comet-observer angle. r_h and Δ are the heliocentric and geocentric distances of the comet during our observations.

as some structures in the form of rays presumably produced by the H_2O^+ doublet at ~6200 Å.

To enhance the existing asymmetries and/or features, two different methods were applied: 1) adaptive Laplace filtering (Richter 1978, 1991; Boehnhardt & Birkle 1994) and 2) radial renormalization (A'Hearn et al. 1986). The former method does not depend on the accuracy of the comet nucleus centering by a 2D Gaussian, and it is more sensitive to gradient changes on different scales depending on the width of the spatial filtering applied. The latter method uses the azimuthally averaged radial profile of the coma flux to create a 2-dimensional image of the average coma flux level and divides it through the original image of the comet.

Figure 1 shows the coma of the comet before and after applying enhancement technique 1 to a median combined image in *R* Bessel. The coma of Comet Lee shows up to four streams or jets (two of them clearly defined) in the anti-sunward direction. These streams are most likely produced by the line doublet at 6198 and 6200 Å of the (0, 8, 0) transition of the $\tilde{A}^2A_1$–$\tilde{X}^2B_1$ electronic system of the H_2O^+, as well as by the comparably strong (0, 6, 0), (0, 7, 0) and (0, 9, 0) bands. These streams have an approximate width of 5° and the two most prominent ones are located at azimuthal angles of 287° and 296° as measured from north toward east.

Ion rays usually occur in pairs on either side of the ion tail, as they trace the magnetic field of the solar wind as it flows through the comet. The flow of the solar wind is decelerated by the addition of cometary ions to the wind. The deceleration is greatest near the nucleus, while on the outer edges of the coma, the solar wind continues to flow near its usual speed. This velocity shear gives the magnetic field lines, and the rays, their "hairpin" shapes.

It is known that significant changes in the ion rays can occurr; they first appear at fairly large angles to the ion tail, typically 45°, and then they brighten and converge towards the tail axis. The faster the solar wind speed at the comet, the more rapid the ion rays move. This process occurs over the course of typically 30 min–1 h. To detect any change in the position angle of the ion rays, and since the comet was imaged during ~45 min, approximately, we have applied a Laplace filtering to the individual images. A slight convergence of the ion rays towards the tail can be seen in Fig. 2. The fact that these variations are not very large indicates that the solar wind speed at the comet might not have been very high at the time of our observations.

The adaptive Laplace filtering, applied to the Gunn *i* images, enhances the ions rays, although their contrast is slightly worse, as expected from a fainter H_2O^+ band at ~7500 Å within the filter bandpass.

The calibration in Af was applied to median combined frames in *R* Bessel and Gunn *i*. The parameter $Af\rho$ was introduced by A'Hearn et al. (1984); it represents a measurement unit related to the dust production rate of a comet. Making use of the available Z_p, we have computed $Af\rho_R \sim 700$ cm and $Af\rho_i \sim 590$ cm at $\rho \approx 40\,000$ km. Note that the bandpass of these filters certainly covers several emissions due to C_2, NH_2, H_2O^+ and CN, besides the solar radiation scattered by the dust, and thus the obtained $Af\rho$ parameters are upper limits to the more realistic ones obtained from the spectroscopic measurements where relatively clean continuum regions can be selected.

3.2. Gas and dust spatial profiles

The gas (NH_2, CN, OI and CI) and dust coma have been studied from the two acquired long-slit spectra in the east-west direction. After flux calibration, both spectra were recentered at the pixel which presumably contains the cometary nucleus and aligned along the slit to the optocenter. The resulting spectrum was then considered to study the CN $A\ ^2\Pi$–$X\ ^2\Sigma^+$ red system, emission bands of NH_2 $\tilde{A}(0, \nu'_2, 0)$–$\tilde{X}(0, 0, 0)$ (hereafter called the "0, ν'_2, 0 band"), atomic oxygen and atomic carbon prompt emissions at 6300/6364 and 9823/9850 Å respectively, as well as the continuum profiles in the east-west direction, dust production rate (as measured from the $Af\rho$ parameter), and approximate size distribution and composition of the cometary dust grains.

Several emission features are visible in both cometary spectra (see Fig. 3, upper panel): the OI(^{1}D) cometary feature at 6300 Å, the NH_2 bands for $\nu'_2 = 9$ (partially), 8, 7, 6 and 5 and the CN red system bands 2–0, 3–1, 1–0 and 2–1. Superimposed on the proper cometary emissions, important telluric bands such as the O_2 B and A, several H_2O and OH bands (longward of 9000 Å) can be seen, as well as the atmospheric oxygen forbidden line at 6300 Å.

To obtain the pure gas emission features, a onedimensional synthetic dust spectrum was obtained using a solar high resolution spectrum (Kurucz et al. 1984) transformed (or calibrated) in flux according to the solar spectrum distribution measured by Labs et al. (1987). This spectrum was convolved with the

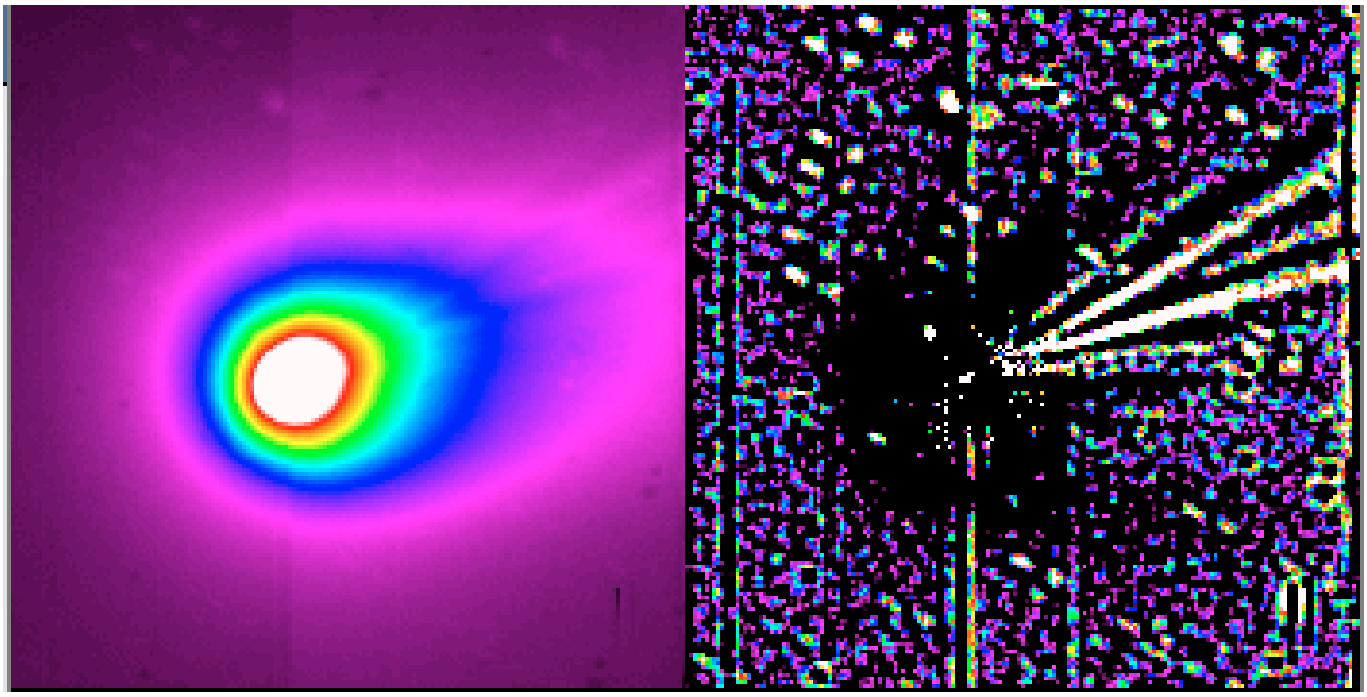

Fig. 1. Comet Lee (C/1999 H1) as imaged in the *R* Bessel filter (*left*) and processed image (Laplace filter with a filter width of 31 pixels) to enhance structures. The angular scale for both images is 4′.58 × 5′.25, which is 200 000 × 230 000 km at the comet distance. North is up and East to the left. Note that up to two clear streams, that are due to H_2O^+, are enhanced by the Laplace filtering. The position angle of these structures is 287° and 296° as measured from north toward east. Each of these features has a width of ~5°. The vertical lines are artifacts from bad columns, whereas the dotty features are background stars.

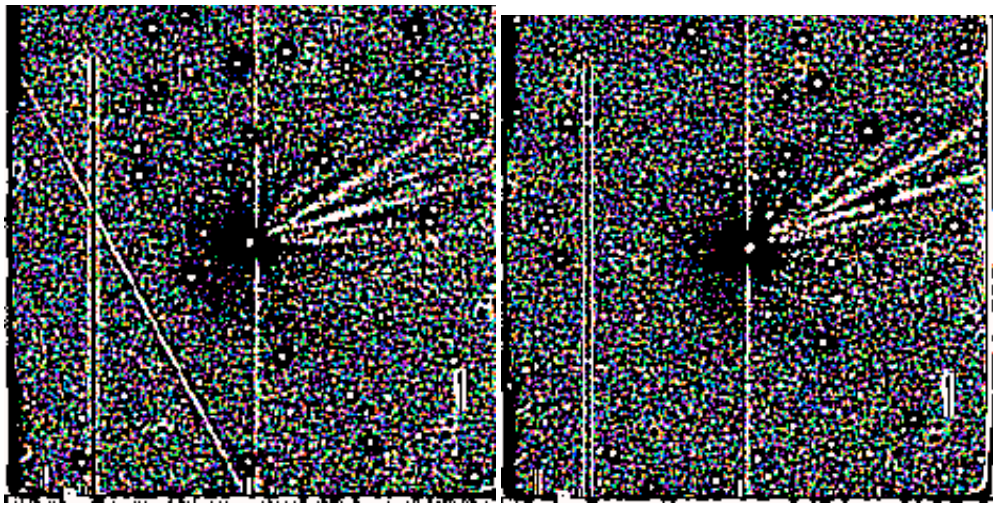

Fig. 2. The ion rays of Comet C/1999 H1 (Lee): images acquired at 23:07:52 UT (*left*) and 23:51:27 UT (*right*) after applying an adaptive Laplace filter (width of 17 pixels). Viewing geometry is as in Fig. 1, whereas the the field of view is 323″.42 × 323″.42 for both frames, which is 280 300 × 280 300 km at the comet distance. Comet nucleus is at the center of the frame. A slight coarsening of the ion rays towards the tail axis can be seen.

instrumental point spread function and adjusted to account for the intrinsic dust color of the comet. The latter is deduced from the slope of the cometary spectrum measured in wavelength regions without known gas contamination. From this, a two dimensional synthetic cometary dust spectrum was created using the cometary dust profiles along the slit, extracted from wavelength regions without gas contamination. Finally, the difference between the cometary and the synthetic dust spectrum gives the cometary gas spectrum. The result can be checked in Fig. 3 where the original cometary spectrum (i.e. the observed one before sky subtraction) and the cometary gas spectrum, both integrated in the spatial direction along the slit, are shown. Note that the cometary gas spectrum, after sky subtraction too, contains practically no telluric lines and/or bands and only the pure cometary gas emissions is visible, that is, the continuum level is about zero. This procedure was applied to each spectrum. After checking the similarity in the intensity of every gas band and/or line in the two spectra, they were median

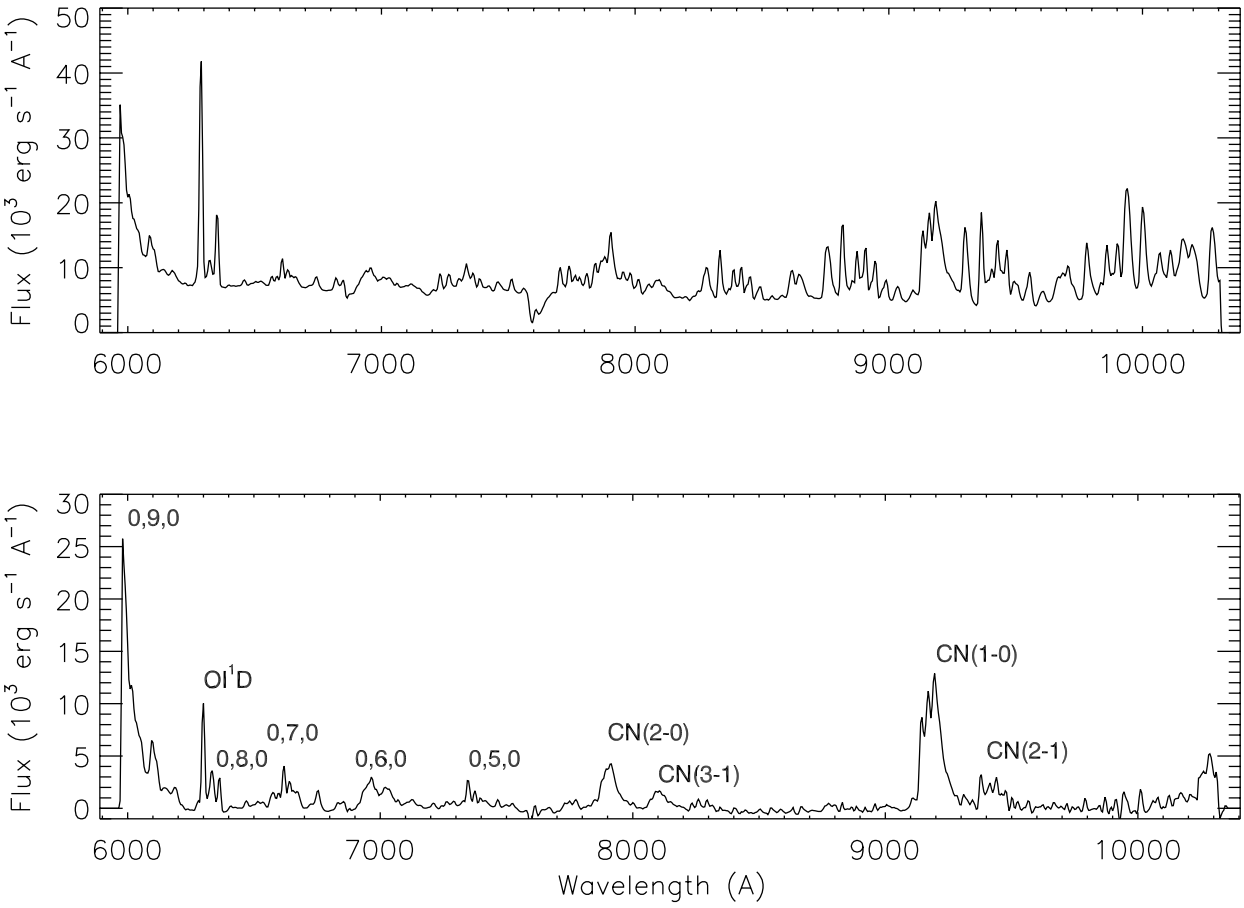

Fig. 3. Observed and gas spectrum of Comet Lee (C/1999 H1) spatially integrated along the slit. In the observed cometary spectrum, the sky values have not been subtracted so that it clearly shows the oxygen telluric line, the O_2 B and A bands at ~6800 and ~7600 Å, H_2O at ~8200 Å, and OH band longward 9000 Å. In the lower panel, pure cometary emissions is seen: the CN red system as well as the (0, ν'_2, 0) NH_2 bands (with the blended OI lines at 6300 Å and at 6364 Å).

combined to increase the S/N. This final spectrum is the one considered for the dust and gas analysis presented in the following sections.

3.2.1. OI + NH_2 and CN

It is widely known that the (0, 8, 0) NH_2 band is blended with the OI(^{1}D) lines, that the (0, 7, 0) is most likely contaminated by the C_2 $\Delta\nu = -3$ sequence, and that the (0, 6, 0) and (0, 5, 0) bands are relatively spread and mixed with strong telluric absorptions. The case of the (0, 8, 0) NH_2 band blended with the oxygen forbidden lines at 6300 and 6364 Å has been previously studied by Fink (1994), Hicks & Fink (1997), and Fink et al. (1999). To properly obtain the NH_2 and OI(^{1}D) uncontaminated flux, both species need to be corrected. High resolution spectra of several comets, including P/Halley (Arpigny et al. 1987a; Combi & McCrosky 1991) show that most of the (0, 8, 0) NH_2 emission consists of a peak centered near 6290 Å, and thus blended with the 6300 Å OI(^{1}D) line, and a pure NH_2 feature centered near 6335 Å, as well as a number of weaker features. The average ratio $\frac{F_{6290}}{F_{6335}}$ for eight comets is about 0.87, while five observations of comet P/Halley at varying heliocentric distance yielded 0.86. This factor was determined by Arpigny et al. (1987b) and it seems to be quite robust over a wide range of geocentric and heliocentric distances, as well as being independent of spectral resolution as long as the OI and the NH_2 peaks can be reasonably well resolved. To obtain the pure 6300 Å OI emission, we thus multiplied the 6335 Å NH_2 peak by this number, and subtracted this amount of NH_2 from the OI + NH_2 blend at 6300 Å. Next, to obtain the total NH_2 flux of the (0, 8, 0) band, the flux measured at 6335 Å was multiplied by 2 since the emission at that wavelength comprises about 0.49 of the total NH_2 flux (see Fink 1994).

Besides the difficulty in extracting pure NH_2 emission from some of the bands appearing in the cometary spectrum (see Fig. 3), the exact resonance fluorescence g-factors are not known. The g-factors for the NH_2 bands commonly used are those in Tegler & Wyckoff (1989) until 1994, and the same g-factors halved later on. This change was required because Arpigny (1995) pointed out that the even bands $\nu'_2 = 8, 6$, etc. and the odd bands $\nu'_2 = 9, 7$, etc., each account for half the population of NH_2 molecules in the ground state. Recently, the NH_2 fluorescence efficiencies have been re-calculated by Kawakita & Watanabe (2002). These authors computed the g-factors as a function of heliocentric distance, finding that the fluorescence efficiencies for even $-\nu'_2$ bands are approximately proportional to r_h^{-n}, where $n = 1.5-1.6$, while those for the odd$-\nu'_2$ bands cannot be approximated by the r_h^{-n} function.

Table 2. CN emission bands extracted from the spectra, their corresponding g-factors, and derived production rates.

Species	Spectral region (Å)	g-factor (erg s^{-1} mol^{-1})	Q (10^{26} s^{-1})
CN(2–0)	7822–8039	2.70×10^{-14}	2.97 ± 0.13
CN(3–1)	8032–8213	9.85×10^{-15}	3.77 ± 0.23
CN(1–0)	9109–9323	8.91×10^{-14}	3.24 ± 0.17
CN(2–1)	9342–9528	2.33×10^{-14}	2.55 ± 0.12
			3.13 ± 0.51[a]

[a] Mean CN production rate on June 6, 1999.

The C_2 contamination of the $\nu'_2 = 7, 6$ NH_2 bands becomes clear when comparing the east-west profiles derived from the (0, 8, 0) band with the (0, 7, 0) and (0, 6, 0) bands: the one deduced from the (0, 8, 0) is noticeably steeper (and more characteristic of arising from NH_3 photodissociation) than the ones resulting either from the (0, 6, 0) or the (0, 7, 0) band which are much flatter, reflecting the contamination by the $\Delta\nu_2 = -3$ C_2 emissions. Therefore, only the NH_2 profile derived from the (0, 8, 0) band will be used for the gas analysis of the coma of Comet Lee. The corresponding g-factor is 3.63×10^{-15} erg s^{-1} mol^{-1} according to Tegler & Wyckoff (1994), or 7.79×10^{-15} erg s^{-1} mol^{-1} as inferred from the data in Table 1 of Kawakita & Watanabe (2002) interpolated at $r_h = 0.98$ AU (heliocentric distance of Comet Lee during our observations).

The CN emission bands in the red system are strongly peaked, with well-defined boundaries and good contrast with respect to the continuum. Thus, their extraction from the cometary gas spectrum is straightforward according to the ranges listed in Table 2. The column densities for each band are derived making use of the g-factors adopted from Fink (1994) and also listed in Table 2.

We have tried to fit the CN and NH_2 column density profiles derived from each band in the east-west direction under the assumption of constant production rates, i.e. a steady state model, by applying the Haser modeling (Haser 1957) with parent expansion velocities given by the expression $v_p = 0.86 \times r_h^{-0.4}$ km s^{-1} (Biver et al. 2000), while v_d is held constant and equal to 1 km s^{-1} for both CN and NH_2. The Haser equivalent (see Combi & Delsemme 1980) scalelengths (l_p, l_d) best fitting the column density profiles are (48 500, 255 000) km for every CN profile. The obtained CN production rates are listed in Table 2. In the case of NH_2, a theoretical profile obtained with $l_p = 7500$ km, $l_d = 70\,000$ km, and production rate $(5.52 \pm 0.03) \times 10^{27}$ s^{-1} (if the g-factor is from Tegler & Wyckoff 1994) or $(1.18 \pm 0.01) \times 10^{27}$ s^{-1} (if the fluorescence factor is from Kawakita & Watanabe 2002) best resembles the observations. Figure 4 shows the observed profiles in the east-west direction together with the theoretical profiles best reproducing the observed ones.

3.2.2. H_2O

The water production rate is derived from the flux measurement of the forbidden O^1D line at 6300 Å. This oxygen line, and the one at 6364 Å, are not produced by resonance fluorescence, but by the prompt emission produced by the photodissociation of H_2O, which directly populates the OI(^{1}D) and OI(^{3}P) states. The reported branching ratio to that channel (8.2% by Festou & Feldman 1981 and 8.3% by Budzien et al.1994) probably has an uncertainty of 20–30%. Due to its short lifetime (~110 s), the O^1D flux profile faithfully traces out the H_2O parent molecule distribution, and its emission is comparatively narrow. From the total luminosity L (in photons s^{-1} m^{-2}) at 6300 Å, and integrating the spectrum of Comet Lee along the full spatial slit length (i.e. $\approx 1 \times 10^5$ km), we have derived a H_2O production rate of $(1.22 \pm 0.7) \times 10^{29}$ s^{-1} for a branching ratio of 8.3% in the process $H_2O + h\nu \rightarrow O(^1D) + H_2$ at $\lambda < 1360$ Å.

3.2.3. CI

The abundance of carbon atoms in the metastable ^{1}D state near the cometary nucleus provides information on one of the main sources of carbon in the cometary coma. The prompt emission of the ^{1}D–^{3}P doublet takes place at 9823/9850 Å. The ^{1}D state of carbon is metastable, with a lifetime of 4077 s (Hibbert et al. 1993), likely produced by CO photodissociation (Tozzi et al. 1998). At the available spectral resolution ($FWHM = 2$ Å), we have searched for the C(^{1}D) doublet at 9823 and 9850 Å. No clear spectral feature was found in the inner coma ($\rho \leq$ 12 250 km, i.e. one "scale length" assuming $\tau \approx 4077$ s and $v_d \approx 3.9$ km, Huebner et al. 1992) at any of these wavelengths. A 3σ flux upper limit for the doublet 9823/9850 Å has been computed to be $(4.56 \pm 0.52) \times 10^{-17}$ erg cm^{-2} s^{-1}.

3.2.4. Dust brightness profiles

The two dimensional cometary dust spectrum has allowed us to study the behavior of the dust and of its color as a function of ρ. Three continuum regions at 6250 Å, 7230 Å and 8900 Å can be selected for the study of the cometary dust. Figure 5 shows the brightness profiles derived from the spectrum for the continua centered at 6250 Å and 8900 Å. All of these profiles, either in east or west direction, can be adequately fit by the law $\log B \sim -m \log \rho$ with $m \sim 1$ (see Table 3). This is consistent with a steady state coma for a constant dust production rate and long-lived grains expanding radially outward, where the spatial number density should decrease as r^{-2}, where r is the nucleocentric distance. Consequently, the projected surface brightness would decrease as ρ^{-m} with $m = 1$.

3.2.5. A f ρ

Estimates of the dust production in comets are usually made by means of the parameter $A(\theta)f\rho$ (A'Hearn et al. 1984). The expression to compute the equivalent radius ρ of a rectangular aperture (as used in our observations) is taken from Roettger (1991), yielding 2.″35 (i.e. 2040 km at the comet distance).

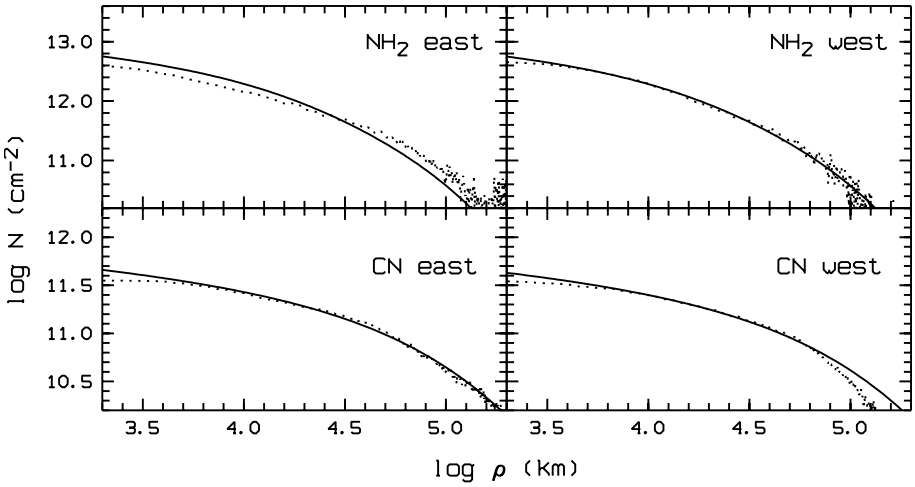

Fig. 4. CN and NH_2 column density profiles of Comet Lee (dots) in the east-west direction. The solid lines represent the results obtained by means of the Haser model with equivalent scalelengths and production rates listed in Table 2 for CN (1–0) and as mentioned in the text for NH_2.

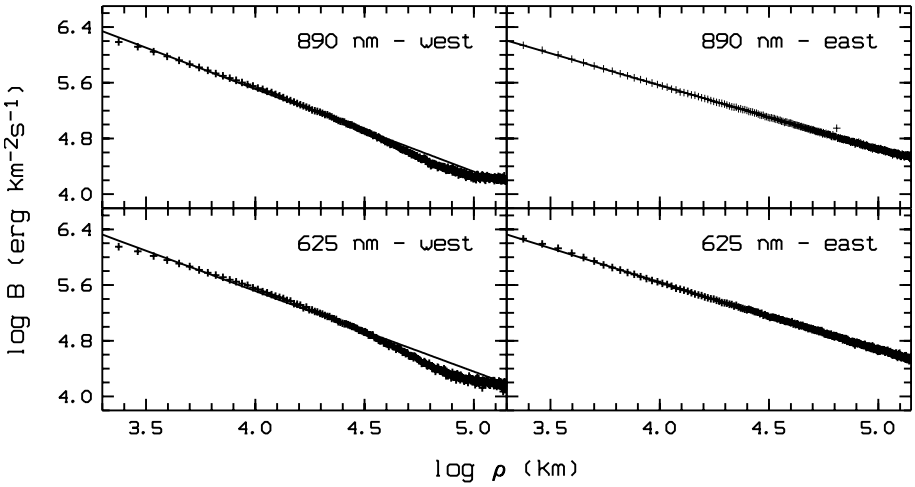

Fig. 5. Brightness profiles of Comet Lee in two different continuum regions. The profiles were obtained from the median averaged spectrum in the east-west direction, representing approximately the sun-tail direction. The surface brightness, B, is plotted against the projected radius, ρ in double logarithmic representation. Dots represent the observed profiles and the solid lines are the best fits verifying $\frac{\mathrm{d}(\log\ B)}{\mathrm{d}(\log\ \rho)} = -m$ starting at $\log\ \rho \geq 3.2$, with slopes listed in Table 3.

Table 3. Slope of linear fits in Fig. 5.

Spectral range (Å)	Slope[a] West	East
6231–6267 (6250)	1.16 ± 0.03	0.978 ± 0.010
6800–6900 (6850)	1.20 ± 0.03	0.966 ± 0.006
7188–7266 (7230)	1.19 ± 0.03	0.917 ± 0.006
8866–8942 (8900)	1.00 ± 0.02	0.718 ± 0.008

[a] Linear fit for the region $3.2 \leq \log \rho \leq 4.6$ (i.e. $1600 \leq \rho \leq 40\,000$ km).

From the flux in the continuum (6800–6900 Å), we have calculated $A(\theta)f\rho = 496$ cm, below the upper limit computed from the broadband images in *R* Bessel and Gunn *i*, as expected.

Following A'Hearn et al. (1995), the gas-to-dust mass ratio can be evaluated by

$$\log\left(\frac{M_{\mathrm{gas}}}{M_{\mathrm{dust}}}\right) = \log\left[Q(\mathrm{OH})/Af\rho\right] - 25.4. \quad (1)$$

According to this expression, and considering the simultaneous Q_{OH} (direct observations by Feldman et al. 1999 at 3085 Å and by Biver et al. 2000 at 18 cm or derived from water production rates as $0.90 \times Q_{\mathrm{H_2O}}$, this work and Neufeld et al. 2000) and the $Af\rho$ parameter here presented (~500 cm), the gas-to-dust mass ratio is bracketed between 6.5 and 11.7 at $r_h = 0.98$ AU.

3.2.6. Dust color

As the long-slit spectrum covers a wide wavelength range, and contains spatial information in approximately Sun-tail direction, the color of the cometary dust vs. the projected cometocentric distance ρ can be easily derived. The bandpass representing continuum emissions are listed in Table 3. After

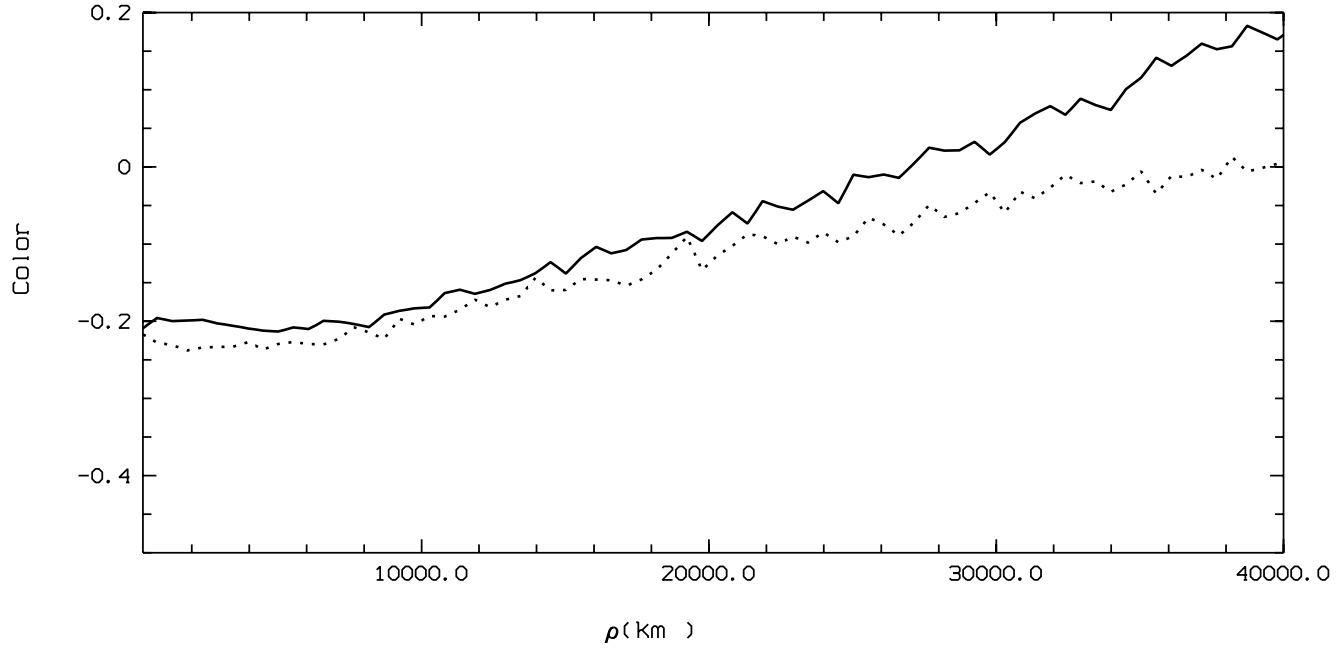

Fig. 6. Color of the dust in the coma of C/1999 H1 (Lee) in the west (solid line) and east (dotted line) direction as computed from Eq. (1) for $8400 \leq \lambda_L \leq 8500$ Å and $6800 \leq \lambda_S \leq 6900$ Å. Note the increasing reddening of the dust at $\rho \geq 10\,000$ km in both directions. At larger cometocentric distances, the differences in east-west direction cannot be attributed to significant variations in the physical and/or chemical properties of the cometary dust since at $\rho > 30\,000$ km the error due to the contribution of the sky is getting larger.

re-centering the spectrum at each wavelength range at the optocenter as determined by fitting a one-dimensional Gaussian to the inner part of the coma, the intensity peaks are all located within a fraction (∼0.2) of a pixel, and the color of the dust is computed as

$$C_{S-L} = \ln\left(\frac{F_L}{F_S}\right) \tag{2}$$

where F_S, F_L are the averaged reflected flux of the cometary dust, as a function of ρ, in the shorter and the longer wavelength ranges, respectively (see Kolokolova et al. 2001).

Regardless of what the continuum bandpass we consider, the color of the dust is rather constant at every ρ in the east and west direction as shown in Fig. 6. In both directions, there seems to be a slight reddening of the cometary dust at increasing ρ from the nucleus. By averaging the cometary emission in two spectral regions free of gas contamination (i.e. λ_L = (8450 ± 50) Å and λ_S = (6850 ± 50) Å), we have also computed an intrinsic reddening of the dust of ∼9% per 1000 Å.

3.2.7. Size distribution and composition of the dust grains

Given this steady behavior of the dust color and of the canonical log $B \approx -1$ log ρ indicating that the dust grains are long-lived while traveling outward, we have tried to obtain some approximate information on the size distribution and likely composition of the dust grains by applying simple Mie-scattering theory (Bohren & Huffman 1983) to a log-normal size distribution (see Hansen & Travis 1974) of homogeneous spherical particles:

$$n(a) = \frac{1}{(2\pi)^{1/2}\sigma_m}\frac{1}{a}\exp\left[-(\ln\ a - \ln\ a_m)^2/\left(2\sigma_m^2\right)\right]. \tag{3}$$

By varying the mean radius a_m, the width of the distribution σ_m and the optical constants (i.e. the complex refractive index $m = n - ik$), we have found that the best agreement (see Fig. 7) between observations and computations is reached for an ensemble of particles whose mean radius is 1 μm, $\sigma_m = 1.5$, with a complex refractive index representative of a mixture of silicates (i.e. modified astronomical silicate) and icy grains ($m = 1.33-0i$).

4. Discussion

The analysis of CCD images and of long-slit spectra of Comet Lee in the red branch of the spectrum has provided morphological and compositional information on the coma of another long-period comet recently visiting the inner Solar System.

The morphological analysis has been carried out on broad-band images. Regarding the dust, besides the spherical coma no other dust features have been found. However, the existence of ion rays becomes quite clear after applying enhancement techniques. These ion rays are mainly produced by the line doublet at 6198 and 6200 Å of the (0, 8, 0) transition of the $\tilde{A}^2A_1$–$\tilde{X}^2B_1$ electron system of H_2O^+. Being usually produced in pairs on either side of the tail at a quite large angle of ∼45° or more, they converge to the tail axis in a relatively short time (∼30–60 min) From the first to the last comet image in *R* Bessel on June 6, 1999, obtained 45 min apart, there

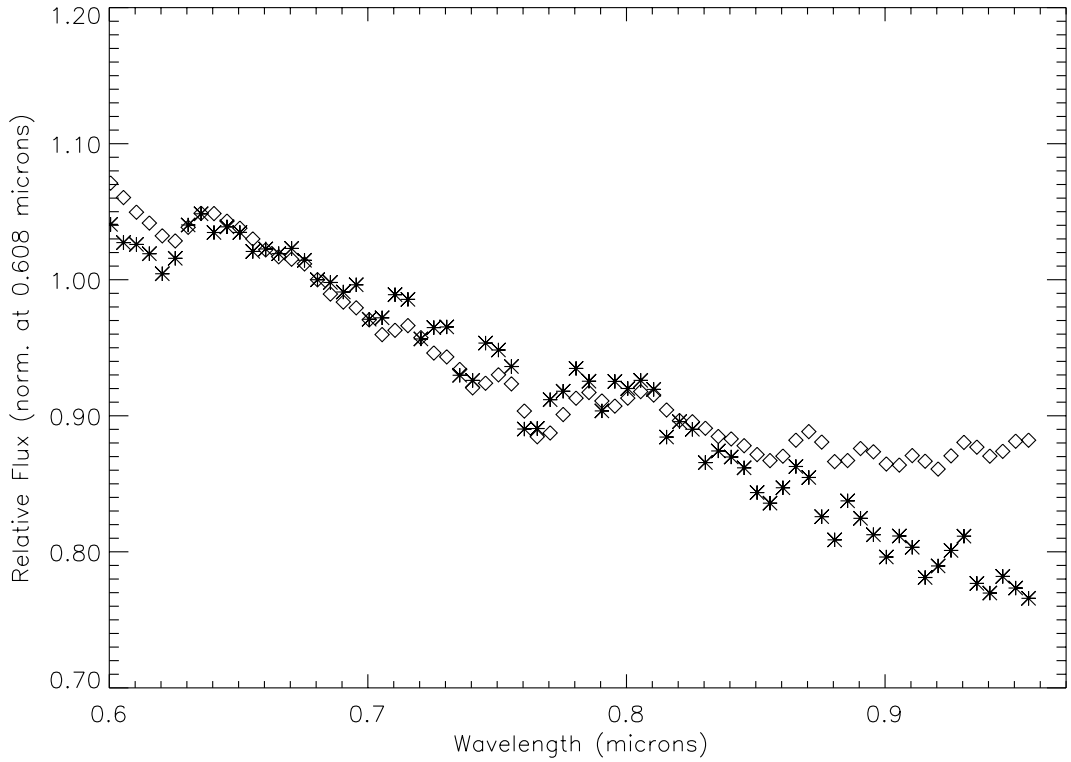

Fig. 7. Comparison between the observed light scattered by the cometary dust in C/1999 H1 (Lee) and that computed by means of the Mie-scattering theory. Data and theoretical results are normalized at 6805 Å. Asterisks refer to observations and diamonds to Mie-theory computations.

was a variation in the position angle of the two most prominent ion rays in ~3°. The lack of images acquired with interference filters (CN, C_2, C_3, OH, etc.) does not allow us to ascertain whether other gas structures are superimposed to the spherical coma. Furthermore, neither the CN nor the NH_2 column density, as derived from the east-west profiles in every band, show any noticeable asymmetry in that particular direction. There is a slight overabundance of NH_2 to the west at cometocentric distances lower than ~20 000 km.

The CN band complex gives relatively consistent results, as seen in Table 2. The production rate derived from the CN (3–1) band is higher than that derived from the other bands, whereas that deduced from the (2–1) band is much lower. As mentioned by Fink (1994), the CN system is mixed with a number of highly variable H_2O bands. More concisely, the CN (2–0) band lies just to the redward continuum region of a strong telluric water band. Furthermore, the published fluorescence efficiencies or g-factors might be affected by an overall uncertainty of ≤20% (Fink 1994). The average CN production rate is $(3.13 \pm 0.51) \times 10^{26}$ s^{-1}, whereas discarding the highest derived CN production rate gives an average value of $(2.92 \pm 0.34) \times 10^{26}$ s^{-1}. In both cases, the error is approximately ≤16%, that is, Q_{CN} can be considered as realistic within the uncertainties derived from the inaccuracy of the g-factors and the calibration errors (note that the airmass of the comet spectrum was very high and that the flux calibration might have suffered from this). The required CN parent Haser equivalent scalelength to fit the observational data (i.e. 48 500 km) together with the assumed parent expansion velocity (~0.86 km s^{-1}) indicates that the lifetime of the CN parent at 1 AU is in the order of 55 000 s, very close to the value deduced by Biver et al. (2000) for the inverse of the HCN photodissociation rate at 1 AU (2.0×10^{-5} s^{-1}) for a moderate to high solar activity. Moreover, the fact that the Q_{CN} presented here and the Q_{HCN} obtained by Mumma et al. (2001) are very similar seems to support the idea that the observed CN might arise only from HCN, and that it is not necessary to invoke the presence of extended sources or other parent molecules beside HCN to explain the CN abundance in the coma of Comet Lee.

The water production rate derived in this work, $(1.22 \pm 0.70) \times 10^{29}$ s^{-1}, can be considered as compatible with other published measurements from OH measurements at 18 cm and/or 3085 Å. Simultaneous to our optical observations, Comet Lee was observed by Biver et al. (2000) in the millimeter range as part of a campaign from May 4 to October 26, 1999. The 18 cm OH lines in the comet were detected on a daily basis at the Nançay Radio Telescope. From 4 transits on 06/04.65–08.63 UT, Biver et al. (2000) deduced an average OH production rate of $(8.8 \pm 0.7) \times 10^{28}$ s^{-1}. Assuming an $H_2O \rightarrow$ OH branching ratio of 90%, the H_2O production rate is $1.1 \times Q_{OH}$, that is ~9.7×10^{28} s^{-1}. For the same date, Feldman et al. (1999) from the OH emission in the UV at 3085 Å deduced a water production rate equal to 1.5×10^{29} s^{-1}, higher by ~55%. Considering the water production rate derived in this work, and that the CN is solely produced by HCN with a branching ratio of 100%, we derive a value for HCN/H_2O of 0.25%, slightly higher than the value deduced by Biver et al. (2000) from simultaneous observations of OH

(and thus H_2O) and HCN (i.e. 0.11 ± 0.02%). Also, this HCN-to-H_2O ratio is about the maximum found by Biver et al. (2002) from a sample of 24 comets studied at radio wavelengths, that were similar to the HCN enriched 109P/Swift-Tuttle or C/1999 O1 (Hale-Bopp). These reported discrepancies (0.25% versus 0.11%) may be due to several factors: (i) Biver et al. (2000) millimeter observations point to a lower gas activity, either in H_2O or HCN, and this is more noticeable in the case of HCN whose production rate is 3 times lower than the one obtained here from the CN red system, (ii) the uncertainties in the flux calibration of the spectra and in the g-factors of the CN red system, (iii) the systematic differences associated with the Haser modeling, and (iv) the well known discrepancy in the H_2O water production rate when derived from the OH mm and 18 cm lines, and OH in the UV or from OI(^{1}D) emission at 6300 Å. Thus, HCN/H_2O ~ 0.27% with a 22% uncertainty. On the other hand, this hydrogen cyanide-to-water ratio drastically decreases if the Submillimeter Waver Astronomy Satellite (SWAS) measurements (Neufeld et al. 2000) are considered, as the H_2O production rate is 50% higher with respect to Nançay data (radio observations of hydroxyl molecules).

The non-detection of the CI(^{1}D) doublet at 9823/9850 Å might arise from the fact that C/1999 H1 (Lee) shows a noticeable depletion in CO as compared to other long-period comets. More concisely, the CO/H_2O is 5–10 times lower than that expected for similar comets (Mumma et al. 2001). Biver et al. (2000) could only set an upper limit for the CO production on UT June 06.1, $Q_{CO} < 5.60 \times 10^{27}$ s^{-1}, whereas on UT August 24.8 $Q_{CO} = (2.6 \pm 0.8) \times 10^{27}$ s^{-1}, meaning CO/H_2O ~ 1.8%. By considering these production rates, CI(^{1}D) column densities profiles can be computed and thus, the energy flux as a function of ρ. For a CO lifetime as the inverse of the photodissociation rate for high solar activity ($J = 1.21 \times 10^{-6}$ s^{-1}), CO ejection velocity of $0.86 r_h^{-0.4}$ km s^{-1}, CI(^{1}D) excess velocity of 3.9 km s^{-1} (Huebner et al. 1992) and lifetime ~4000 s, the vectorial modeling (Festou 1981) predicts CI column densities ranging from 2.29×10^{10} cm^{-2} and $<1.77 \times 10^{11}$ cm^{-2} at ρ ~ 10 000 km, depending on the assumed CO production rate. Taking into account that the transition probability for the forbidden line $^1D_2 - ^3P_2$ (9850 Å) within the ground state configuration of CI is 1.8×10^{-4} s^{-1} (Czyzak & Poirier 1985; Hibbert et al. 1993; Tozzi et al. 1998), these CI(^{1}D) column densities would result into 1.7×10^{-18} erg cm^{-2} s^{-1} and $<1.3 \times 10^{-17}$ erg cm^{-2} s^{-1}, below the 3σ flux upper limit measured in our observations. The CO production rate on June 6, 1999 as derived from the 3σ upper limit of CI infrared doublet, is $\leq 5.75 \times 10^{28}$ s^{-1}, an order of magnitude higher than previous determinations by Biver et al. (2000).

Spectroscopic observations of NH_2 give hints on the ammonia abundance in comets. The photolytic reaction for photodissociation of ammonia $NH_3 + h\nu \rightarrow NH_2 + H$ has a 95% quantum yield. Therefore, provided that NH_3 is the dominant source of NH_2, the abundance of the latter is essentially a direct measurement of the ammonia abundance in comets. However, as Meier et al. (1994) have noted, the NH_3/H_2O deduced from spectroscopic measurements of NH_2 gives systematically very low, i.e. in a factor of ~2, ammonia-to-water ratios or present considerable scatter. The ammonia measurements carried out in situ for comet P/Halley by the Giotto spacecraft indicate that this discrepancy can be as high as one order of magnitude. The ammonia-to-water abundance for Comet Lee ranges from ~1% to ~4% depending on the considered g-factors, viz. those given by Kawakita & Watanabe (2000) or Tegler & Wyckoff (1989) corrected according to Arpigny (1995), respectively. This ammonia-to-water ratio is slightly higher than the Q_{NH_3}/Q_{H_2O} reported for other long-period comets, either old or dynamically new (see Feldman et al. 1993), placing the ratio between 0.4% and 0.8% within a factor of 2, and more recently for Comet Hyakutake (0.3%) derived by Palmer et al. (1996), whereas it is closer to the estimates in Meier et al. (1994) from the Giotto flyby measurements and to the predictions by gas coma photochemical models (Allen et al. 1987).

Our estimate of the gas-to-dust mass ratio indicates that C/1999 H1 can be considered as a relatively dust poor comet. The behaviour of the dust grains, as deduced from the study of the log B vs. log ρ points to a steady-state and isotropic outflow of the solid cometary component composed of long-lived grains. The quantitative composition and size distribution of these grains can be inferred from Mie-scattering modeling. The observed spectrum in the range 6000–10 000 Å can be fitted by a dust grain population of silicates and icy grains whose mean radius is ~1 μm. Some discrepancies between observations and modeling are seen beyond 8700 Å likely due to the use of constant (i.e. non-wavelength dependent) refractive index of the dust material. For our spectroscopic range, the real part of the complex refractive index for representative cometary material can be considered constant with wavelength, whereas the imaginary part shows noticeable variations not taken into account in our computations. Regardless of what the continuum bandpass we consider, the color of the dust is almost constant at every ρ in east and west direction, only showing a steady reddening at increasing ρ from the nucleus in both directions. At distances higher than 25 000 km, the differences between the east and west direction are likely due to the approximate 2D sky subtraction and not to real east-west differences in the dust population.

Although Comet Lee was not extensively monitored, the available observations of this comet have provided us with a new opportunity for studying the behaviour of another long-period comet lately visiting the inner Solar System. From a general point of view, Comet Lee, C/1999 H1 can be considered as a rather depleted CO comet, whereas it is considerably abundant in CH_3OH according to Biver et al. (2000). In this respect, comet C/1999 H1 is intrinsically different from C/1995 O1 (Hale-Bopp) and C/1996 B2 (Hyakutake), although the three comets are thought to have a common origin. Regarding carbon-chain species, the abundance of ethane and acetylene with respect to that of water, (~0.6 and ~0.3, respectively) is much the same for the three comets (Mumma et al. 2001). The optical data obtained at ESO also allow us to compare Comet Lee with some of the comets presented in the surveys by A'Hearn et al. (1995) and Fink & Hicks (1996). Comparison of the log of the production rates ratios $\frac{CN}{OH}$ and $\frac{Af\rho}{OH}$ for comet C/1999 H1 with the values for the restricted data set in Table 4 of A'Hearn et al. (1995) indicates that Comet Lee is similar to periodic comets 23P/Brorsen-Metcalf,

6P/d'Arrest or 2P/Encke and to long period comets such as Okazaki-Levy-Rudenko (C/1989 Q1), Thiele (C/1985 T1) or Sugano-Saigusa-Fujigawa (C/1983 J1). It should be noted that the previously mentioned comets all bear the characteristic of being "typical" within the taxonomy introduced by A'Hearn et al. (1995), that is, $\log \frac{Q(C_2)}{Q(CN)} \geq -0.18$, and for all of them this ratio lies between –0.09 and 0.29. This characteristc also seems to be present in Comet Lee as $\log \frac{Q(C_2)}{Q(CN)} \sim 0.28$, that is, the abundance of carbon-chain species (C_2) can be considered as typical, assuming that either acetylene or ethane are the only precursors of C_2 with 100% efficiency.

Similarly, of the 39 comets surveyed by Fink & Hicks (1996), comet C/1999 H1 resembles comets 73P/Schwassmann-Wachmann 3 or 2P/Encke in terms of CN to H_2O relative abundance. Comparison of the NH_2 content versus H_2O in the same database is more uncertain given the new results on the g-factors by Kawakita & Watanabe (2002). Previous studies (Fink 1994; Fink & Hicks 1996; Hicks & Fink 1997; Fink et al. 1999) showed that there is some dependency on the heliocentric distance for the NH_2 abundance; namely, the NH_2-to-H_2O ratio becomes larger for larger r_h. The new determination of the NH_2 fluorescence efficiency (as a function of r_h) removes this dependency, giving rise to NH_2-to-H_2O ratios nearly constant within the range from 0.5 to 3 AU. Basing our comparison on the NH_2 production rates derived by means of the most recent g-factors (i.e. Kawakita & Watanabe 2002), the NH_2/H_2O, and thus ammonia-to-water ratio, in comet C/1999 H1 (Lee) is ∼1%, consistent with what was found for 1P/Halley, C/1996 B2 (Hyakutake) and C/1996 O1 (Hale-Bopp), that is, 0.5%, 0.6% and 1.5%, respectively.

5. Summary

Long-slit spectrophotometric observations of Comet Lee (C/1999 H1) were acquired on June 6, 1999. For slit acquisition and pointing purposes, several comet images were obtained with R Bessel and Gunn i filters. The morphological anaylsis of these images has unveiled the presence of two pairs of ion rays slowly converging to the tail axis during the 45 min the comet was imaged. As the comet was not observed in interference filters, the existence of dust and/or neutral gas structures cannot be ascertained.

CN and NH_2 column densities have been derived from the long-slit spectra. The Q_{CN} and Q_{NH_2} production rates have been obtained by means of the Haser model yielding to $\sim 3 \times 10^{26}$ s^{-1} and $\sim 1 \times 10^{27}$ s^{-1}, respectively. The water production rate $Q_{H_2O} \sim 1.22 \times 10^{29}$ s^{-1}, inferred from the luminosity of the OI(^{1}D) line at 6300 Å is in reasonable agreement with values reported by Biver et al. (2000) and by Feldman et al. (1999) on the same date. The CI(^{1}D) doublet at 9823/9850 Å, indicative of the CO abundance in C/1999 H1, has not been undoubtedly detected, only 3σ upper limit flux emission $\sim 4 \times 10^{-17}$ erg cm^{-2} s^{-1}, that is $Q_{CO} < 5.78 \times 10^{28}$ s^{-1}, has been inferred. The ratios of HCN and NH_3 to H_2O are ∼0.28% and ∼1%, in agreement with what has been obtained for other long-period comets.

The $Af\rho$ parameter, a measure related to the dust production rate, is relatively low (∼500 cm) allowing us to classify this comet as a poor dust comet with a gas-to-dust mass ratio in the range between 6 and 12 depending on the measurements that provide the OH (and thus, water) production rate. The dust brightness profiles in east-west direction do not deviate from the canonical law $\log B \sim m \log \rho$ with $m = 1.01 \pm 0.16$, whereas the dust slightly reddens with distance from the nucleus. The dust grain population can be characterised by a relatively broad size distribution whose solid particles have a quite common mean radius of 1 μm and are composed of a mixture of silicates and icy grains.

Although the organic volatile composition of the long period comet C/1999 H1 (Lee) very much resembles that of other long period comets (such as Hyakutake or Hale-Bopp) pointing to a common origin and/or evolution, other peculiarities are also present in some Jupiter family comets such as 2P/Encke, 6P/d'Arrest or 73P/Schwassmann-Wachmann 3, or in 1P/Halley, a long-period and dynamically old comet. For a more meaningful characterisation of comet Lee, a wider covering of its behaviour as a function of the heliocentric distance would have been desirable. However, given the available information and in the current state, Jupiter family comets with likely origin in the Kuiper Belt, Halley-type comets and long-period comets presumably coming from the Oort Cloud do not show clearly distinct compositions.

Acknowledgements. L.M.L is grateful to G. H. Jones for fruitful conversations on ion rays. The research carried out has been partially supported by the Spanish Ministerio de Ciencia y Tecnología under contracts PNE-002/2000-C and PNE-001/2000-C-01.

References

A'Hearn, M. F., Schleicher, D. G., Millis, R. L., Feldman, P. D., & Thompson, D. T. 1984, AJ, 89, 579
A'Hearn, M. F., Hoban, S., Birch, P. V., et al. 1986, Nature, 324, 649
A'Hearn, M. F., Millis, R. L., Schleicher, et al. 1995, Icarus, 118, 223
Allen, M., Delitsky, M., Huntress, W., et al. 1987, A&A, 187, 502
Arpigny, C., Magain, P., Manfroid, J., et al. 1987a, AJ, 187, 485
Arpigny, C., Manfroid, J., Magain, P., et al. 1987b, ESA SP–278, 571
Arpigny, C. 1995, ASP Conf. Ser., 177, 71
Biver, N., Bocklée-Morvan, D., Crovisier, J., et al. 2000, AJ, 120, 1554
Boehnhardt, H., & Birkle, K. 1994, A&A, 107, 101
Bohren, C. F., & Hufmann, D. R. 1983, in Absorption and scattering of light by small particles (New York: Wiley)
Budzien, S. A., Festou, M. C., & Feldman, P. D. 1994, Icarus, 107, 164
Chiu, K., Neufeld, D. A., Bergin, E. A., et al. 2001, Icarus, 154, 345
Combi, M. R., & Delsemme, A. H. 1980, ApJ, 237, 633
Combi, M. R., & McCrosky, R. E. 1991, Icarus, 91, 270
Czyzak, S. J., & Poirier, C. P. 1985, Ap&SS, 116, 21
Feldman, P., Fournier, K. B., Grinin, V. P., & Zvereva, A. M. 1993, ApJ, 404, 348
Feldman, P. D., Weaver, H. A., A'Hearn, M. F., et al. 1999, BAAS, 31, 1127
Festou, M. C. 1981, A&A, 95, 69
Festou, M., & Feldman, P. 1981, A&A, 103, 154
Fink, U. 1994, ApJ, 423, 461
Fink, U., & Hicks, M. D. 1996, ApJ, 459, 729
Fink, U., Hicks, M. D., & Fevig, R. A. 1999, Icarus, 141, 331
Hansen, J. E., & Travis, L. D. 1974, Space Sci. Rev., 16, 527
Haser, L. 1957, Bull. Cl. Sci. Acad. R. Belg., 43, 740

Hibbert, A., Biemont, E., Godefroid, M., & Vaeck, N. 1993, A&AS, 99, 179
Hicks, M. D., & Fink, U. 1997, Icarus, 127, 307
Huebner, W. F., Keady, J. J., & Lyon, S. P. 1992, Adv. Space Sci., 195, 1
Huebner, W. F., & Link, R. 1999, http://espsun.space.swri.edu/spacephysics/atomic/html/photoabs.htm
Kawakita, H., & Watanabe, J. 2002, ApJ, 572, L177
Kolokolova, L., Lara, L. M., Schulz, R., Stüwe, J. A., & Tozzi, G. P. 2001, Icarus, 153, 197
Kurucz, R. L., Furenlid, I., Brault, J., & Testerman, L. 1984, National Solar Observatory Atlas, No. 1, June 1984
Labs, D., Neckel, H., Simon, P. C., & Thuiller, G. 1987, Sol. Phys., 90, 25
Meier, R., Eberhardt, P., Krankowsky, D., & Hodges, R. R. 1994, A&A, 287, 268
Melnick, G. J., Gary, J., Stauffer, J. R., et al. 2000, ApJ, 539, L77
Mumma, M. J., McLean, I. S., DiSanti, M. A., et al. 2001, ApJ, 546, 1183
Neufeld, D. A., Stauffer, J. R., Bergin, E. A., et al. 2000, ApJ, 539, L151
Palmer, P., Wooten, A., Butler, B., et al. 1996, BAAS, 188, 62.12
Richter, G. M. 1978, Astron. Nachr., 299, 283
Richter, G. M. 1991, Proc. 3rd ESO Workshop on Data Analysis, 37
Roettger, E. E. 1991, Ph.D. Thesis, John Hopkins University, Baltimore, Maryland
Tegler, S., & Wyckoff, S. 1989, ApJ, 343, 445
Tozzi, G. P., & Licandro, J. 2002, Icarus, 157, 187
Tozzi, G. P., Feldman, P. D., & Festou, M. C. 1998, A&A, 330, 753
Weaver, H. A., et al. 1999, BAAS, 31, 1123
Womack, M., Stern, S. A., & Festou, M. C. 1997, Planet. Space. Sci., 45, 711